Journal of Computational Physics 235 (2013) 497–514

Contents lists available at SciVerse ScienceDirect

Journal of Computational Physics

journal homepage: www.elsevier.com/locate/jcp

A minimum action method for small random perturbations of two-dimensional parallel shear flows

Xiaoliang Wan *

Department of Mathematics and Center for Computation and Technology, Louisiana State University, Baton Rouge, LA 70803, United States

ARTICLE INFO

Article history:
Received 30 March 2012
Received in revised form 5 October 2012
Accepted 8 October 2012
Available online 30 October 2012

Keywords:
Random perturbation
Dynamical system
White noise
Minimum action method
Rare events
Spectral elements
Finite elements

ABSTRACT

In this work, we develop a parallel minimum action method for small random perturbations of Navier–Stokes equations to solve the optimization problem given by the large deviation theory. The Freidlin–Wentzell action functional is discretized by *hp* finite elements in time direction and spectral methods in physical space. A simple diagonal preconditioner is constructed for the nonlinear conjugate gradient solver of the optimization problem. A hybrid parallel strategy based on MPI and OpenMP is developed to improve numerical efficiency. Both *h*- and *p*-convergence are obtained when the discretization error from physical space can be neglected. We also present preliminary results for the transition in two-dimensional Poiseuille flow from the base flow to a non-attenuated traveling wave.

1. Introduction

Dynamical systems are often subject to random perturbations since noise is ubiquitous in nature. Even when these random perturbations have a small amplitude, they can produce a profound effect on the long time dynamics by inducing rare but important events. A large number of interesting phenomena in physics, chemistry and biology such as phase transitions, biological switches and chemical reactions, etc., are examples of such noise-induced rare events [13].

When the random perturbations are small, the Freidlin–Wentzell theory of large deviations provides a rigorous mathematical framework for us to understand how the transitions occur and how frequent they are. The transition pathways between metastable sets in a dynamical system often have a rather deterministic nature. As the noise amplitude decreases to zero, the events for successful transitions between metastable sets have a sharply peaked probability around a certain deterministic path that is least unlikely. Special features of such a path tell us crucial information about the mechanism of the transition, which is closely related to the structure of the phase space. One class of examples that have been well studied for a long time are the gradient systems, for which the vector field is the gradient of a potential function. In gradient systems, the most probable transition path is the minimum energy path (MEP), which passes through the basin boundary between the stable states at some saddle points with one dimensional unstable manifold [16,21]. For non-gradient systems we need to consider the action functional instead of the energy, which is the central object to the Freidlin–Wentzell theory. The minimizer of the action functional provides the most probable transition path; the minimum of the action functional provides an estimate of the probability and the rate of occurrence of the transition. Thus an important practical task is to compute the minimum and minimizer of the action functional. A large number of algorithms have been designed for gradient systems.

* Tel.: +1 2255786367.
E-mail address: xlwan@math.lsu.edu

0021-9991/$ - see front matter © 2012 Elsevier Inc. All rights reserved.
http://dx.doi.org/10.1016/j.jcp.2012.10.006

Some popular algorithms include the string method [3,5], nudged elastic band method [12], eigenvector- following-type method (e.g.[1]) as well as the dimer method [11], which usually take advantage of the fact that in gradient systems the transition paths are always parallel to the drift term of the stochastic differential equation. For general (non-gradient) systems, we need to minimize directly the Freidlin–Wentzell action functional and available algorithms include the minimum action method (MAM) [4], the adaptive MAM [19], the geometric MAM [10] and a high-order MAM [23].

In this work, we focus on the minimum action method for small random perturbations of Navier–Stokes equations. In particular, we are interested in whether the minimum action method can provide a new strategy to study the nonlinear instability of parallel shear flows. Stability of parallel shear flows, including plane Poiseuille flow, plane Couette flow, pipe flow, etc., is still a challenging dynamical problem, which people are not able to fully understand it through linear, (weakly) nonlinear and non-modal stability theories. In particular, the mechanism of the transition from the laminar flow to turbulence is still an open problem. Recently, people start to pay attention to study this problem by using an optimization strategy, where nonlinearity is included into the defined objective function. For example, in [15], the most dangerous initial perturbation leading to the turbulence state in plane Couette flow is examined by maximizing the time-averaged dissipation for a certain energy level of the initial disturbance. We look at this problem from a probabilistic point of view. Thinking of the Navier–Stokes equations perturbed by small noise, there exists a positive probability that a transition occurs from the laminar state to another state (including a turbulence state). By the Freidlin–Wentzell theory, an optimal path (or minimal action path) can be given by the minimizer of the Freidlin–Wentzell action functional, which describes the least unlikely route from the laminar state to the new state. We are interested in the intermediate states along this path. Since the minimal action path is closely related to the structure of the basin of attraction of the base flow [21,20,22], we expect to get useful information about the nonlinear instability along the minimal action path. As the first step of such a strategy, we develop the algorithm of the minimum action method for the stochastic Navier–Stokes equations.

This paper is organized as follows. We first describe the Freidlin–Wentzell theory for small random perturbations of dynamical systems in Section 2. A general methodology for the minimum action method of stochastic partial differential equations is given in 3. We develop the minimum action method for the stochastic Navier–Stokes equations in section 4. We include some numerical results for two-dimensional Poiseuille flows in Section 5, followed by a summary section.

2. Theoretical background

Although we are interested in the random perturbations of Navier–Stokes equations in this work, which are stochastic partial differential equations, we use stochastic differential equations to present the theoretical background of minimum action method for simplicity and without loss of generality. Let the random process $X_t = X(t) : \mathbb{R}_+ \to \mathbb{R}^n$ defined by the following stochastic ordinary differential equation (SODE):

$$dX_t = b(X_t)dt + \sqrt{\varepsilon}dW_t, \tag{1}$$

where W_t is a standard Wiener process in $\mathbb{R}^n$ and ε is a small positive parameter. Let $\phi(t) \in \mathbb{R}^n$ be an absolutely continuous function defined on $t \in [0, T]$. The Freidlin–Wentzell theory [7] tells us that the probability of $X(t)$ passing through the δ-tube about ϕ on $[0, T]$ is

$$\Pr(\rho(X, \phi) < \delta) \approx \exp\left(-\frac{1}{\varepsilon} S_T(\phi)\right), \tag{2}$$

where $\rho(\phi, \varphi) = \sup_{t\in[0,T]}|\phi(t) - \varphi(t)|$, and $S_T(\phi)$ is the action functional of ϕ on $[0, T]$, defined as

$$S_T(\phi) = \frac{1}{2}\int_0^T L(\dot{\phi}, \phi)dt, \tag{3}$$

where $L(\dot{\phi}, \phi) = |\dot{\phi} - b(\phi)|^2$. In general, we have the following large deviation principle

$$\lim_{\varepsilon\to 0} \varepsilon \log \Pr(X \in A) = -\min_{\phi\in A} S_T(\phi), \tag{4}$$

where A is a subset of the path space. Hence, in analogy with the Laplace's method, the basic contribution to $\Pr(X \in A)$ is given by the neighbourhood of the minimum of $S_T(\phi)$ when ε is small enough, in the sense that away from the minimizer of the action functional $S_T(\phi)$ the probability that the event A occurs through other possible choices will decay exponentially. The minimizer ϕ^*, which satisfies $S_T(\phi^*) = \min_{\phi\in A} S_T(\phi)$ is also called the "minimal action path" (MAP).

Different definitions of the set A in Eq. (4) correspond to many important phenomena that occur in dynamical systems. For example, if we are interested in the transition from one point a_1 to the other point a_2 in the phase space on the time interval $[0, T]$ due to small random perturbations, A can be defined as

$$A = \{\phi(t)|\phi(0) = a_1,\ \phi(T) = a_2\}.$$

The MAP will be the most probable path for the transition from a_1 to a_2 where the probability of the system taking all the other paths decays exponentially with respect to the noise amplitude ε according to the large deviation principle. Note that when a_1 and a_2 are attractors, it is more appropriate to define the set A as

$$A = \{\phi(t) | \phi(-\infty) = a_1,\ \phi(\infty) = a_2\}.$$

We keep a finite time interval here mainly due to the numerical approximation discussed later. If a_1 and a_2 are two adjacent stable states in gradient systems, the MAP will be consistent with the minimum energy path (MEP), which passes through the basin boundary between a_1 and a_2 at a certain saddle point with one-dimensional unstable manifold. If there exists dynamics between a_1 and a_2, the MAP will be the path given by the dynamics corresponding to a zero action functional, which implies that the MAP is also helpful for us to study the structure of the phase space. For instance, if a_1 and a_2 are two unstable fixed points and the MAP has a zero action functional, we can conclude that there exists a heteroclinic orbit between a_1 and a_2.

Although the Freidlin–Wentzell theory shows that it is very important to find out the MAP when we consider small random perturbations of dynamical systems, it is usually very difficult to obtain it analytically for a general dynamical system. We need to consider numerical approximation in practice.

3. A general methodology of MAM for SPDE

Several minimum action methods have been proposed for non-gradient dynamical systems, see [4,19,10,23]. The method proposed in this work is an extension of the minimum action method proposed in [23]. Consider the random perturbations of the following general partial differential equation on a physical domain $D \subset \mathbb{R}^d, d = 1, 2, 3$:

$$\frac{\partial u(\mathbf{x}, t)}{\partial t} = \mathcal{G}u(\mathbf{x}, t) + \sqrt{\varepsilon}\dot{W}(\mathbf{x}, t), \tag{5}$$

where $\mathbf{x} \in D, \mathcal{G}$ indicates a differentiation operator in physical space, and $\dot{W}(\mathbf{x}, t)$ is space–time white noise. The action functional on the time interval $[0, T]$ for the SPDE (5) is defined as [6]

$$S_T(u) = \frac{1}{2}\int_0^T \int_D (\partial_t u - \mathcal{G}u(\mathbf{x}, t))^2 d\mathbf{x}dt = \frac{1}{2}\langle \partial_t u - \mathcal{G}u, \partial_t u - \mathcal{G}u\rangle_{\mathbf{x},t}, \tag{6}$$

where $\langle f, g\rangle_{\mathbf{x},t}$ is the inner product of f and g with respect to both $\mathbf{x}$ and t. We are interested in the minimizer $u^*(\mathbf{x})$ of $S_T(u)$:

$$S_T(u^*) = \min_{u \in A} S_T(u), \tag{7}$$

where A is a set of paths in the phase space subject to the constraints

$$u(\mathbf{x}, 0) = u_0(\mathbf{x}), \quad u(\mathbf{x}, T) = u_T(\mathbf{x}). \tag{8}$$

We first look at the Euler–Lagrange equation of the optimization problem (7). Define the linear perturbation operator $\hat{\mathcal{G}}$ as

$$\mathcal{G}(u + \delta u) = \mathcal{G}u + \hat{\mathcal{G}}\delta u + O(\delta^2 u), \tag{9}$$

where δu is a perturbation function. Consider the functional derivative of S_T, which satisfies

$$\delta S_T(u) = \left\langle \frac{\delta S_T(u)}{\delta u}, \delta u \right\rangle_{\mathbf{x},t} = \lim_{\epsilon \to 0} \frac{S_T(u + \epsilon\delta u) - S_T(u)}{\epsilon}. \tag{10}$$

It is easy to obtain that

$$\delta S_T(u) = S_T(u + \delta u) - S_T(u) = \left\langle \frac{\delta S_T}{\delta u}, \delta u \right\rangle_{\mathbf{x},t} = \langle \partial_t u - \mathcal{G}u, \partial_t \delta u - \hat{\mathcal{G}}\delta u\rangle_{\mathbf{x},t}, \tag{11}$$

where all high-order terms with respect to δu are neglected. Thus the functional derivative of $S_T(u)$ takes the form

$$\frac{\delta S_T}{\delta u} = (\partial_t - \hat{\mathcal{G}})^*(\partial_t - \mathcal{G})u, \tag{12}$$

where $(\partial_t - \hat{\mathcal{G}})^*$ is the adjoint operator of $\partial_t - \hat{\mathcal{G}}$. In other words, the Euler–Lagrange equation of $S_T(u)$ is

$$\begin{cases} (\partial_t - \hat{\mathcal{G}})^*(\partial_t - \mathcal{G})u = 0, & \mathbf{x} \in D,\ t \in [0, T] \\ u(\mathbf{x}, 0) = u_0(\mathbf{x}), & \mathbf{x} \in D \\ u(\mathbf{x}, T) = u_T(\mathbf{x}), & \mathbf{x} \in D \\ \text{Boundary Conditions} & \mathbf{x} \in \partial D \end{cases} \tag{13}$$

Since $\mathcal{G}$ is a nonlinear operator, the Euler–Lagrange equation (13) is also nonlinear. Furthermore, if $\mathcal{G}$ has a differentiation order of k in physical space, $(\partial_t - \hat{\mathcal{G}})^*(\partial_t - \hat{\mathcal{G}})$ will be a $2k$th order operator in $\mathbf{x}$ and a second-order operator in t, corresponding to a $(d+1)$-dimensional nonlinear boundary value problem. For a general methodology, we consider the numerical approximation of the optimization problem (7) instead of discretizing equation (13) directly.

Let $\{h_i(\mathbf{x})\}_{i=1}^{N_\mathbf{x}}$ and $\{\psi_i(t)\}_{i=1}^{N_t}$ span the approximation spaces for physical space and time, respectively. Then $u(\mathbf{x}, t)$ has the following approximation

$$u(\mathbf{x},t) \approx u_h(\mathbf{x},t) = \sum_{i=1}^{N_{\mathbf{x}}}\sum_{j=1}^{N_t} u_{ij} h_i(\mathbf{x})\psi_j(t). \tag{14}$$

The optimization problem (7) has the following discrete version

$$S_T(u_h^*) = \min_{\substack{u_{ij}\in\mathbb{R} \\ i=1,\ldots,N_{\mathbf{x}};\, j=1,\ldots,N_t}} S_T(u_h), \tag{15}$$

subject to a proper discretization of the constraints at $t = 0, T$ and on ∂D. It is well known that the key part of almost all efficient optimization algorithms is the computation of the gradient. We now derive a general formula for the gradient $\partial S_T/\partial u_{ij}$. In the approximation space, the perturbation function can be expressed as

$$\delta u_h(\mathbf{x},t) = \sum_{i=1}^{N_{\mathbf{x}}}\sum_{j=1}^{N_t} \delta u_{ij} h_i(\mathbf{x})\psi_j(t). \tag{16}$$

Noticing that

$$\delta S_T(u_h) = \left\langle \frac{\delta S_T(u_h)}{\delta u}, \delta u_h \right\rangle = \sum_{i=1}^{N_{\mathbf{x}}}\sum_{j=1}^{N_t} \left\langle \frac{\delta S_T(u_h)}{\delta u}, h_i(\mathbf{x})\psi_j(t) \right\rangle_{\mathbf{x},t} \delta u_{ij}, \tag{17}$$

and combining Eqs. (11) and (17), we obtain the gradient of S_T

$$\frac{\partial S_T}{\partial u_{ij}} = \left\langle \frac{\delta S_T(u_h)}{\delta u}, h_i(\mathbf{x})\psi_j(t) \right\rangle_{\mathbf{x},t} = \left\langle (\partial_t - \mathcal{G})u_h, (\partial_t - \hat{\mathcal{G}})h_i(\mathbf{x})\psi_j(t) \right\rangle_{\mathbf{x},t}. \tag{18}$$

Here we assume that the basis functions $h_i(\mathbf{x})$ and $\psi_j(t)$ have the regularity required by the operators $\mathcal{G}$ and $\hat{\mathcal{G}}$. Once the gradient of the action functional is obtained, we can choose an appropriate optimization solver to minimize the action functional $S_T(u_h)$. In this work, we consider the nonlinear conjugate gradient method.

Remark 1. $u_0(\mathbf{x})$ and $u_T(\mathbf{x})$ are often chosen as steady states given by

$$\mathcal{G}u(\mathbf{x}) = 0, \tag{19}$$

while the MAP is a solution of the Euler–Lagrange equation (13). Since the spatial differentiation order of $(\partial_t - \hat{\mathcal{G}})^*(\partial_t - \mathcal{G})$ is twice as large as that of $\mathcal{G}$, the basis functions for the approximation of $(\partial_t - \hat{\mathcal{G}})^*(\partial_t - \mathcal{G})$ demands more regularity than those for $\mathcal{G}$, which implies that the basis functions for the approximation of $u(\mathbf{x})$ in Eq. (19) may be not appropriate for the MAP if the action functional is discretized without any modification. For example, assume $\mathcal{G}$ is of second order. If we employ the finite element method to solve Eq. (19), basis functions $h_i(\mathbf{x}) \in H^1(D)$ can be used. However, the Euler–Lagrange equation (13) require basis functions $h_i(\mathbf{x}) \in H^2(D)$ within the continuous Galerkin framework. Since we are interested in the channel flow in this work, which has a simple geometry and can be discretized efficiently by the spectral method, such an issue is avoided naturally.

3.1. Numerical efficiency of MAM

Considering that parallel computing is the most straightforward way to enhance the numerical efficiency, especially for large scale simulations, we here present a general discussion about the parallelization of the minimum action method. More details can be found in [24].

First of all, we observe that $S_T(u)$ is a nonlinear functional of u and $\mathcal{G}$ is, in general, a nonlinear operator in physical space, which implies that it can be difficult to consider parallelization, e.g., domain decomposition, in space, especially when spectral methods are employed for the physical discretization. Thus, we do not consider the parallelization of operator $\mathcal{G}$.

To make the parallelization in the time direction more efficient, we choose $\{\psi_i(t)\}_{i=1}^{N_t}$ as the *hp* finite element basis [14], which consists of piecewise polynomials. We define the standard basis functions on the reference element $[-1,1]$ as:

$$\hat{\psi}_k(\tau) = \begin{cases} \frac{1-\tau}{2} & k = 0, \\ \frac{1-\tau}{2}\frac{1+\tau}{2}P_{k-1}^{1,1}(\tau), & 0 < k < p, \\ \frac{1+\tau}{2} & k = p, \end{cases} \tag{20}$$

where $P_k^{1,1}(\tau)$ denote orthogonal Jacobi polynomials of degree k with respect to the weight function $(1-\tau)(1+\tau)$. It is seen that $\hat{\psi}_0(\tau)$ and $\hat{\psi}_p(\tau)$ are consistent with linear finite element basis, and $\hat{\psi}_k(\tau)$, $0 < k < p$, are introduced for high-order approximation. Note that $\hat{\psi}_k(\pm 1) = 0$ for $0 < k < p$. We call $\hat{\psi}_0(\tau)$ and $\hat{\psi}_p(\tau)$ boundary modes, and $\hat{\psi}_k(\tau), 0 < i < p$, interior modes. For a partition $t_0 = 0 < t_1 < t_2 < \cdots < t_{N_e} = T$ of the interval $[0,T]$, where N_e is the number of elements, the local basis functions $\psi_i(t)$ in each element $[t_m, t_{m+1}]$ will be obtained through an affine mapping as $\psi_i(t) = \psi_{i(m,k)}(t) = \hat{\psi}_k(\tau_m(t))$, where

we treat the global index i as a function of $m = 1, \ldots, N_e$ and $k = 0, \ldots, p$, and $t = \tau_m^1(\tau) = \frac{t_{m+1}-t_m}{2}\tau + \frac{t_{m+1}+t_m}{2}$ when $t \in [t_m, t_{m+1}]$. Based on such a choice of the finite element basis, i.e., $\psi_{i(m,k)}(t) = 0$ on element boundaries for $0 < k < p$, only the coefficients of $\psi_{i(m,0)}$ or $\psi_{i(m,p)}$ need to be exchanged between two adjacent CPU processors when we distribute the time elements to different processors. Also a good scalability can be achieved even if different polynomial orders are employed in each element. However, since we only parallelize one direction, i.e., the time direction, we have a limit for the number of processors, which is equal to the number of time elements. Thus, extra parallelization in each time element is desired for more numerical efficiency, because the number of degrees of freedom from the physical discretization can be large.

We observe that the most time-consuming part in the optimization algorithm is the computation of the gradient. Furthermore, each component of the gradient $\partial S_T/\partial u_{i,j}$ can be regarded as a functional of the basis function $h_i(\mathbf{x})\psi_j(t)$ according to Eq. (18), where the computation of these functionals are independent of each other once we obtain $\partial_t u - \mathcal{G}u$. In other words, the computation of the gradient $\nabla S_T(u)$ can be further parallelized providing that $\partial_t u - \mathcal{G}u$ is available.

To this end, we identify two favourable structures of the MAM for parallel computing. The first one is the parallelization of time elements, where the information of the boundary modes needs to be shared. The second one is the parallelization of the computation of the gradient within each time element, where the information about $\partial_t u - \mathcal{G}u$ needs to be shared. Such a two-level parallelism actually agrees very well with the typical computer architecture for high performance computing (HPC), e.g., a multi-core symmetric multiprocessing cluster. Modern HPC systems usually consist of computation nodes which have multi-core processors, where the processor cores on the same computation node can share the memory and work independently.

Summarizing the above discussions, we present our hybrid MPI/OpenMP strategy: (1) We distribute the time elements uniformly to a certain number of computation nodes, which can be done by MPI. Here we assume that the same polynomial order is used for all time elements. (2) For a certain computation node, we distribute the components of gradient $\nabla S_T(u)$ uniformly to all processor cores after $\partial_t u - \mathcal{G}u$ is obtained, which can be done by OpenMP. In a nutshell, we use MPI across computation nodes and OpenMPI within computation nodes, corresponding to the natural two-level parallelism of our minimum action method. Numerical experiments for the performance of such a hybrid parallel strategy are reported in [24]. We also note that such a hybrid strategy can also be achieved by coupling MPI and GPU for more numerical efficiency.

4. Minimum action method for stochastic Navier–Stokes equations

We consider the two-dimensional incompressible Navier–Stokes (N–S) equations perturbed by small divergence-free space–time white noise:

$$\begin{cases} \frac{\partial \mathbf{u}}{\partial t} + (\mathbf{u}\cdot\nabla)\mathbf{u} = -\nabla p + \frac{1}{Re}\Delta\mathbf{u} + \sqrt{\varepsilon}\dot{W}(\mathbf{x},t), \\ \nabla\cdot\mathbf{u} = 0, \end{cases} \tag{21}$$

where $\mathbf{u} = (u, v) \in \mathbb{R}^2$, $Re = \frac{U\mathrm{h}}{\nu}$ is the Reynolds number, U is the velocity at $y = 0$, and ν is the dynamic viscosity. We define the physical domain $D := [0, 2\pi] \times [-\mathrm{h}, \mathrm{h}]$, where h is a positive real number.

For convenience, we decompose the velocity and pressure field into two parts:

$$\mathbf{u}_{\mathrm{tot}} = \mathbf{u}_b + \mathbf{u}, \quad p_{\mathrm{tot}} = p_b + p,$$

where $\mathbf{u}_b$ and p_b corresponds to the base flows, and from now on $\mathbf{u}$ and p indicate the deviation from the base flows. For the plane Poiseuille flow,

$$\mathbf{u}_b = (1 - (y/\mathrm{h})^2, 0), \quad p_b = -\frac{2}{Re}\frac{x}{\mathrm{h}^2}. \tag{22}$$

For the plane Couette flow,

$$\mathbf{u}_b = (y/\mathrm{h}, 0), \quad p_b = 0. \tag{23}$$

The original stochastic N–S equations can be rewritten as

$$\begin{cases} \frac{\partial \mathbf{u}}{\partial t} + (\mathbf{u}_{\mathrm{tot}}\cdot\nabla)\mathbf{u}_{\mathrm{tot}} = -\nabla p + \frac{1}{Re}\Delta\mathbf{u} + \sqrt{\varepsilon}\dot{W}, \\ \nabla\cdot\mathbf{u} = 0 \end{cases} \tag{24}$$

with boundary conditions

$$\begin{cases} \mathbf{u}|_{x=0} = \mathbf{u}|_{x=2\pi}, \\ p|_{x=0} = p|_{x=2\pi}, \\ \mathbf{u}|_{y=\pm\mathrm{h}} = 0. \end{cases} \tag{25}$$

The action functional for the stochastic N–S Eqs. (24) can be rewritten as

$$S_T(\mathbf{u}, p) = \frac{1}{2}\int_0^T \left\| \frac{\partial \mathbf{u}}{\partial t} + (\mathbf{u}_{\mathrm{tot}}\cdot\nabla)\mathbf{u}_{\mathrm{tot}} + \nabla p - \frac{1}{Re}\Delta\mathbf{u} \right\|_2^2 dt, \tag{26}$$

where $\|\cdot\|$ indicates the L_2 norm in physical space. We then consider the optimization problem

$$S_T(\mathbf{u}^*, p^*) = \min_{(\mathbf{u},p)\in A} S_T(\mathbf{u}, p), \tag{27}$$

subject to the divergence free condition $\nabla \cdot \mathbf{u} = 0$ and the constraints given by the boundary conditions (25), where A is a certain set of paths in the configuration space of N–S equations.

4.1. Choice of the action functional

The main difference of the MAM for N–S equations from our general methodology discussed in Section 3 is that the N–S equations are subject to a divergence-free constraint. Let Π denote the Helmholtz projection operator onto the divergence-free space. Given any $\mathbf{u} \in L_2(D, \mathbb{R}^2)$, there exists a unique $q \in H^1(D)$ with $\int_D q d\mathbf{x} = 0$ such that $\Pi\mathbf{u} = \mathbf{u} + \nabla q$ satisfying

$$0 = (\Pi\mathbf{u}, \nabla\phi) = (\mathbf{u} + \nabla q, \nabla\phi), \quad \forall \phi \in H^1(D), \tag{28}$$

where $\Pi\mathbf{u} \cdot \mathbf{n} = 0$ on ∂D. The Helmholtz decomposition (28) is then associated with an elliptic problem

$$\Delta q = -\nabla \cdot \mathbf{u}, \tag{29}$$

subject to the boundary condition $\frac{\partial q}{\partial \mathbf{n}} = 0$. If we take the Helmholtz projection of the momentum equation, theoretical study [18] shows that the action functional can be written as

$$S_T(\mathbf{u}) = \frac{1}{2}\int_0^T \left\| \frac{\partial \mathbf{u}}{\partial t} + \Pi\left((\mathbf{u}_{\text{tot}} \cdot \nabla)\mathbf{u}_{\text{tot}} - \frac{1}{Re}\Delta\mathbf{u} \right) \right\|_2^2 dt, \tag{30}$$

where the pressure term disappears and the constraint of incompressibility is taken care of by the Helmholtz projection. If we minimize the action functional in the form (30), it is obvious that in each iteration step of an optimization algorithm, at least two Helmholtz projections are needed to obtain $\Pi\mathbf{u}$ and $\Pi((\mathbf{u}_{\text{tot}} \cdot \nabla)\mathbf{u}_{\text{tot}})$, which can be done by solving the associated elliptic problems (29). We also note that the projection might introduce extra errors due to inappropriate boundary conditions for the corresponding elliptic equations. In this work, we consider the action functional of the primitive variables, i.e., Eq. (26). Note that when the divergence-free condition $\nabla \cdot \mathbf{u} = 0$ is satisfied, we have

$$S_T(\mathbf{u}, p) = \frac{1}{2}\int_0^T \left\| \frac{\partial \mathbf{u}}{\partial t} + \Pi\mathbf{Q}(\mathbf{u}) \right\|_2^2 + \|(\mathcal{I} - \Pi)\mathbf{Q}(\mathbf{u}) + \nabla p\|_2^2 dt,$$

where $\mathbf{Q}(\mathbf{u}) = (\mathbf{u}_{\text{tot}} \cdot \nabla)\mathbf{u}_{\text{tot}} - \frac{1}{Re}\Delta\mathbf{u}$ and $\mathcal{I}$ is the identity operator. When the action functional $S_T(\mathbf{u}, p)$ reaches its (local) minimum, we should obtain that

$$\|(\mathcal{I} - \Pi)\mathbf{Q}(\mathbf{u}) + \nabla p\|_2 = 0, \tag{31}$$

due to the uniqueness of the Helmholtz decomposition. In other words, we let the optimization algorithm deal with the Helmholtz projection of $\mathbf{Q}(\mathbf{u})$.

4.2. Definition of the approximation space

In the time direction, we consider a (nonuniform) partition $\mathcal{T}_h$:

$$t_0 = 0 < t_1 < t_2 < \cdots < t_{N_e+1} = T.$$

We employ *hp* finite element basis functions defined by Eq. (20) in time direction, i.e.

$$\psi_i(t) = \psi_{i(m,k)}(t) = \hat{\psi}_k(\tau_m(t)), \tag{32}$$

where the global index $i = 1, \ldots, N_t$ is a function of $m = 1, \ldots, N_e$ and $k = 0, \ldots, p$, and $t = \tau_m^{-1}(\tau) = \frac{t_{m+1}-t_m}{2}\tau + \frac{t_{m+1}+t_m}{2}$ for $t \in [t_m, t_{m+1}]$.

Due to the simple geometry of the physical domain, we employ the spectral method in physical space. For x direction, Fourier expansion is employed for both $\mathbf{u}$ and p because of the periodic boundary conditions. We order the cosine and sine functions as

$$f_0(x) = 1, \quad f_n(x) = \begin{cases} \cos\left(\frac{n+1}{2}x\right), & \text{if} \quad \text{mod}(n,2) = 1, \\ \sin\left(\frac{n}{2}x\right), & \text{if} \quad \text{mod}(n,2) = 0. \end{cases}$$

To deal with the constraint $\mathbf{u}|_{y=\pm \mathrm{h}} = 0$, we choose the basis functions for the y direction as

$$\theta_m(y) = \begin{cases} P_m(y/\mathrm{h}) - P_{m+2}(y/\mathrm{h}), & \text{for } \mathbf{u}, \\ P_m(y/\mathrm{h}), & \text{for } p, \end{cases} \tag{33}$$

where $P_m(y)$ is the Legendre polynomial of order m. It is easy to see that $\theta_m(\pm\mathrm{h}) = 0$, which implies that no-slip boundary conditions for $\mathbf{u}$ in y direction are automatically satisfied.

Then the 2D basis functions for the physical space can be defined as

$$h_{i(m,n)}(\mathbf{x}) = h_{m,n}(x,y) = \theta_m(y) f_n(x), \quad m,n = 0,1,2,\ldots, \tag{34}$$

and $\mathbf{u}$ and p can be approximated as

$$\mathbf{u} \approx \mathbf{u}_h = \sum_{\boldsymbol{\alpha}\in\mathcal{J}} \sum_{i=1}^{N_t} \mathbf{u}_{\boldsymbol{\alpha},i} h_{\boldsymbol{\alpha}}(x,y)\psi_i(t), \tag{35}$$

$$p \approx p_h = \sum_{\boldsymbol{\alpha}\in\mathcal{J},|\boldsymbol{\alpha}|>0} \sum_{i=1}^{N_t} p_{\boldsymbol{\alpha},i} h_{\boldsymbol{\alpha}}(x,y)\psi_i(t), \tag{36}$$

where $N_t \in \mathbb{N}, \mathcal{J} = \{\boldsymbol{\alpha} = (\alpha_1,\alpha_2) | \alpha_1 \leqslant N_x, \alpha_2 \leqslant N_y, N_x, N_y \in \mathbb{N}_0\}$ is a set of two-dimensional indices, and the condition $|\boldsymbol{\alpha}| = \alpha_1 + \alpha_2 > 0$ for p is due to the constraint $\int_D p d\mathbf{x} = 0$ and the orthogonality of Legendre polynomials and Fourier modes.

4.3. Divergence-free constraint

Due to the particular choice of the approximation space for velocity, the no-slip boundary conditions at $y = \pm\mathsf{h}$ are automatically satisfied, i.e., $\mathbf{u}_h|_{y=\pm\mathsf{h}} = 0$. However, $\mathbf{u}_h$ may not be divergence free. Then a projection of $\mathbf{u}_h$ onto the divergence-free space is expected, which can be given by the Helmholtz decomposition $\Pi\mathbf{u}_h = \mathbf{u}_h + \nabla q$. However, $\Pi\mathbf{u}_h$ will introduce a non-zero slip velocity at the boundary $y = \pm\mathsf{h}$, since the Helmholtz decomposition only requires $\Pi\mathbf{u}_h \cdot \mathbf{n} = 0$ instead of $\Pi\mathbf{u}_h = 0$ at $y = \pm\mathsf{h}$. Thus if we project $\Pi\mathbf{u}_h$ onto the approximation space $\{h_{m,n}(x,y)\}$ for velocity, the projection will not be divergence free any more due to the slip velocity $\Pi\mathbf{u}_h \cdot \mathbf{e}_x \neq 0$ at $y = \pm\mathsf{h}$. So we have to consider how the divergence-free constraint affect the velocity in the approximation space.

Let $\mathbf{u}_h^i = (u_h^i, v_h^i)$ indicate the coefficients of $\psi_i(t)$, i.e.

$$u_h = \sum_{i=1}^{N_t} u_h^i(x,y)\psi_i(t), \quad v_h = \sum_{i=1}^{N_t} v_h^i(x,y)\psi_i(t). \tag{37}$$

For any time t, the divergence-free condition is satisfied

$$\nabla\cdot\mathbf{u}_h = \sum_{i=1}^{N_t} (\nabla\cdot\mathbf{u}_h^i)\psi_i(t) = 0,$$

which implies that

$$\nabla\cdot\mathbf{u}_h^i = 0, \quad i = 1,\ldots,N_t. \tag{38}$$

Consider the expansions of u_h^i and v_h^i

$$u_h^i(x,y) = u_0^i(y) + \sum_{n=1}^{N_x/2} u_n^{i,c}(y)\cos(nx) + \sum_{n=1}^{N_x/2} u_n^{i,s}(y)\sin(nx),$$
$$v_h^i(x,y) = v_0^i(y) + \sum_{n=1}^{N_x/2} v_n^{i,c}(y)\cos(nx) + \sum_{n=1}^{N_x/2} v_n^{i,s}(y)\sin(nx),$$

where N_x is assumed to be an even integer. Eq. (38) implies that

$$(v_0^i)' + \sum_{n=1}^{N_x/2} ((v_n^{i,c})' + n u_n^{i,s})\cos(nx) + \sum_{n=1}^{N_x/2} ((v_n^{i,s})' - n u_n^{i,c})\sin(nx) = 0, \tag{39}$$

which results in

$$\begin{cases} (v_0^i)'(y) = 0, \\ (v_n^{i,c})'(y) + n u_n^{i,s}(y) = 0, \\ (v_n^{i,s})'(y) - n u_n^{i,c}(y) = 0. \end{cases} \tag{40}$$

Since there does not exist a constant mode in the approximation space for velocity, we have $v_0^i(y) = 0$. $v_n^{i,c}$ and $v_n^{i,s}$ can be expressed as

$$v_n^{i,c}(y) = \int_{-\mathsf{h}}^{y} -n u_n^{i,s}(\tau)d\tau, \quad v_n^{i,s}(y) = \int_{-\mathsf{h}}^{y} n u_n^{i,c}(\tau)d\tau. \tag{41}$$

It is obvious that $v_n^{i,c}(-\mathsf{h}) = v_n^{i,s}(-\mathsf{h}) = 0$. Let

$$u_n^{i,c}(y) = \sum_{k=0}^{N_y-1} u_{n,k}^{i,c}\theta_k(y), \quad u_n^{i,s}(y) = \sum_{k=0}^{N_y-1} u_{n,k}^{i,s}\theta_k(y),$$

where $\theta_k(y) = P_k(y/\mathrm{h}) - P_{k+2}(y/\mathrm{h})$. Note here that the highest basis mode for $u_n^{i,c}(y)$ and $u_n^{i,s}(y)$ is $\theta_{N_y-1}(y)$ because $v_n^{i,c}(y)$ and $v_n^{i,s}(y)$ are expressed as integrals of $u_n^{i,s}(y)$ and $u_n^{i,c}(y)$, respectively. Using the orthogonality of Legendre polynomials, we have

$$v_n^{i,c}(\mathrm{h}) = \int_{-\mathrm{h}}^{\mathrm{h}} -nu_n^{i,s}(\tau)d\tau = -2n\mathrm{h}u_{n,0}^{i,s},$$
$$v_n^{i,s}(\mathrm{h}) = \int_{-\mathrm{h}}^{\mathrm{h}} nu_n^{i,c}(\tau)d\tau = 2n\mathrm{h}u_{n,0}^{i,c},$$

which implies that $u_{n,0}^{i,c} = u_{n,0}^{i,s} = 0,\ n = 1,\ldots,N_x/2$.

To this end, we obtain the restriction of the divergence-free condition on the degree of freedom in velocity: for $i = 1,2,\ldots,N_t$,

- $v_0^i(y) = 0$.
- $u_{n,0}^{i,c} = u_{n,0}^{i,s} = 0,\ n = 1,\ldots,N_x/2$.
- The highest basis mode for $u_n^{i,c}(y)$ and $u_n^{i,s}(y)$ is $\theta_{N_y-1}(y)$ in contrast to $\theta_{N_y}(y)$ for $v_n^{i,c}(y)$ and $v_n^{i,s}(y)$.

Then the expansion coefficients of $v_h^i(y)$ can be obtained directly from the expansion coefficients of $u_h^i(y)$ through equation (41) such that the divergence-free condition is satisfied exactly.

To this end, all constraints, including the divergence-free constraint and boundary conditions for the velocity, are automatically satisfied by choosing a particular from of the basis functions and explicitly expressing the divergence-free condition through the coefficients of velocity. In other words, the optimization problem (27) becomes an unconstrained one.

Remark 2. Due to the explicit application of the continuity equation, we require that the number of cosine modes in the approximation space is the same as the number of sine modes. Such a requirement is not necessary, in general, for Fourier spectral methods to approximate a PDE solution, where there usually exists one extra cosine mode in the approximation space.

4.4. Gradient of $S_T(\mathbf{u}_h, p_h)$

We first present a general discussion without taking into account the divergence-free constraint. We define the linear operator $\mathcal{L}$ and nonlinear operator $\mathcal{N}$

$$\mathcal{L}(\mathbf{u}_h, p_h) = -\nabla p_h + \frac{1}{Re}\Delta\mathbf{u}_h, \quad \mathcal{N}(\mathbf{u}_h, \mathbf{v}_h) = (\mathbf{u}_h\cdot\nabla)\mathbf{v}_h, \tag{42}$$

whose perturbation operators are

$$\hat{\mathcal{L}}(\delta\mathbf{u}_h, \delta p_h) = -\nabla\delta p_h + \frac{1}{Re}\Delta\delta\mathbf{u}_h, \tag{43}$$
$$\hat{\mathcal{N}}(\delta\mathbf{u}_h, \delta\mathbf{v}_h) = (\delta\mathbf{u}_h\cdot\nabla)\mathbf{v}_h + (\mathbf{u}_h\cdot\nabla)\delta\mathbf{v}_h. \tag{44}$$

Let

$$\mathcal{G}(\mathbf{u}_h, p_h) = \mathcal{L}(\mathbf{u}_h, p_h) - \mathcal{N}(\mathbf{u}_{\mathrm{tot},h}, \mathbf{u}_{\mathrm{tot},h}) \tag{45}$$
$$\hat{\mathcal{G}}(\delta\mathbf{u}, \delta p_h) = \hat{\mathcal{L}}(\delta\mathbf{u}_h, \delta p_h) - \hat{\mathcal{N}}(\delta\mathbf{u}_{\mathrm{tot},h}, \delta\mathbf{u}_{\mathrm{tot},h}), \tag{46}$$

where $\delta\mathbf{u}_{\mathrm{tot},h} = \delta\mathbf{u}_h$ although $\mathbf{u}_{\mathrm{tot},h} \neq \mathbf{u}_h$. We then have the action functional

$$S_T(\mathbf{u}_h, p_h) = \frac{1}{2}\langle\partial_t\mathbf{u}_h - \mathcal{G}(\mathbf{u}_h, p_h), \partial_t\mathbf{u}_h - \mathcal{G}(\mathbf{u}_h, p_h)\rangle_{\mathbf{x},t} \tag{47}$$

and its perturbation

$$\delta S_T(\mathbf{u}_h, p_h) = \langle\partial_t\mathbf{u}_h - \mathcal{G}(\mathbf{u}_h, p_h), \partial_t\delta\mathbf{u}_h - \hat{\mathcal{G}}(\delta\mathbf{u}_h, \delta p_h)\rangle_{\mathbf{x},t}. \tag{48}$$

The gradient $\nabla S_T(\mathbf{u}_h, p_h)$ then takes the form (see Eq. (18))

$$\begin{cases} \left(\frac{\partial S_T}{\partial \mathbf{u}_{\boldsymbol{\alpha},i}}\right)_1 = \delta S_T(\mathbf{u}_h, p_h)|_{\delta\mathbf{u}_h = \mathbf{e}_x h_{\boldsymbol{\alpha}}(x,y)\psi_i(t), \delta p_h = 0}, \\ \left(\frac{\partial S_T}{\partial \mathbf{u}_{\boldsymbol{\alpha},i}}\right)_2 = \delta S_T(\mathbf{u}_h, p_h)|_{\delta\mathbf{u}_h = \mathbf{e}_y h_{\boldsymbol{\alpha}}(x,y)\psi_i(t), \delta p_h = 0}, \\ \frac{\partial S_T}{\partial p_{\boldsymbol{\alpha},i}} = \delta S_T(\mathbf{u}_h, p_h)|_{\delta\mathbf{u}_h = 0, \delta p_h = h_{\boldsymbol{\alpha}}(x,y)\psi_i(t)}, \end{cases} \tag{49}$$

where $\mathbf{e}_x = (1,0)$ and $\mathbf{e}_y = (0,1)$.

According to the discussions in Section 4.3, the vertical velocity $v_h^i(x,y)$ can be regarded as a function of the horizontal velocity $u_h^i(x,y)$ when the divergence-free constraint is applied. Thus we only need to look at the expansion coefficients of $u_h^i(x,y)$:

$$u_h^i = u_0^i(y) + \sum_{n=1}^{N_x/2} u_n^{i,c}(y)\cos(nx) + \sum_{n=1}^{N_x/2} u_n^{i,s}(y)\sin(nx) = \sum_{k=0}^{N_y} u_{0,k}^i \theta_k(y) + \sum_{n=1}^{N_x/2}\sum_{k=1}^{2N_y-1} u_{n,k}^{i,c}\theta_k(y)\cos(nx) + \sum_{n=1}^{N_x/2}\sum_{k=1}^{2N_y-1} u_{n,k}^{i,s}\theta_k(y)\sin(nx).$$

Since $u_0^i(y)$ is not affected by the divergence-free constraint, we have

$$\frac{\partial S_T}{\partial u_{0,k}^i} = \delta S_T(\mathbf{u}_h, p_h)|_{\delta\mathbf{u}_h = \mathbf{e}_x\theta_k(y)\psi_i(t), \delta p_h = 0}. \tag{50}$$

We now look at $\partial S_T/\partial u_{n,k}^{i,c}$. Let $\delta u_h(x,y) = \delta u_{n,k}^{i,c}\theta_k(y)\cos(nx)$. According to Eq. (41), we must have

$$\delta v_h(x,y) = \delta u_{n,k}^{i,c}\left(\int_{-h}^{y} n\theta_k(\tau)d\tau \sin(nx)\right) \tag{51}$$

correspondingly, which also contributes to $\partial S_T/\partial u_{n,k}^{i,c}$. Thus

$$\frac{\partial S_T}{\partial u_{n,k}^{i,c}} = \delta S_T(\mathbf{u}_h, p_h)|_{\delta\mathbf{u}_h = (\theta_k(y)\cos(nx)\psi_i(t), n\int_{-h}^{y}\theta_k(\tau)d\tau\sin(nx)\psi_i(t)), \delta p_h = 0}. \tag{52}$$

Similarly, we have

$$\frac{\partial S_T}{\partial u_{n,k}^{i,s}} = \delta S_T(\mathbf{u}_h, p_h)|_{\delta\mathbf{u}_h = (\theta_k(y)\sin(nx)\psi_i(t), -n\int_{-h}^{y}\theta_k(\tau)d\tau\cos(nx)\psi_i(t)), \delta p_h = 0}. \tag{53}$$

Remark 3. To compute the gradient component exactly, we need $2(N_x+1)$ quadrature points in x direction and $2N_y+4$ Gauss–Lobatto quadrature points in y direction. Otherwise, we will have aliasing errors. The effect of the aliasing errors will be studied numerically. To reduce the computation cost, we would initially employ N_x+1 quadrature points in x direction and N_y+3 points in y direction. If necessary, we can increase the number of quadrature points.

4.5. Optimization solver

Once the gradient of the action functional is computed, we use the nonlinear conjugate gradient (CG) method to solve the optimization problem to get the MAP $(\mathbf{u}_h^*, p_h^*)$. Let $\mathbf{\Phi} \in \mathbb{R}^{N_{\mathbf{x},t}}$ be a global vector whose components are unknown coefficients of $\mathbf{u}_h$ and p_h, where $N_{\mathbf{x},t}$ indicates the total number of degrees of freedom. The nonlinear CG method can be summarized as

$$\begin{cases} \mathbf{\Phi}_{k+1} = \mathbf{\Phi}_k + \alpha_k \mathbf{d}_k, \\ \mathbf{d}_{k+1} = -\mathbf{g}_{k+1} + \beta_k^{\mathrm{HZ}}\mathbf{d}_k, \quad \mathbf{d}_0 = -\mathbf{g}_0, \end{cases} \tag{54}$$

where the subscript k indicates the iteration step, the positive step size α_k is obtained by a line search algorithm, $\mathbf{g}_k = \nabla S_T(\mathbf{\Phi}_k)$, and β_k^{HZ} is the CG update parameter. We define $\beta_k^{\mathrm{HZ}} = \max\{\beta_k, \eta_k\}$ as in [9]

$$\beta_k = \left(\mathbf{y}_k - \mathbf{d}_k\frac{|\mathbf{y}_k|^2}{\mathbf{d}_k^{\mathrm{T}}\mathbf{y}_k}\right)^{\mathrm{T}}\frac{\mathbf{g}_{k+1}}{\mathbf{d}_k^{\mathrm{T}}\mathbf{y}_k}, \ \eta_k = \frac{-1}{|\mathbf{d}_k|\min\{0.01, |\mathbf{g}_k|\}} \tag{55}$$

with $\mathbf{y}_k = \mathbf{g}_{k+1} - \mathbf{g}_k$.

To accelerate the convergence of CG iteration, an efficient preconditioner is desired, which is usually problem dependent for a nonlinear objective function. In [22,23], we used the inverse of the linear part of the Euler–Lagrange equation as a preconditioner for the nonlinear CG solver, which was demonstrated to be efficient for the Kuramoto–Sivashinsky equation. Such a strategy can also be applied to the N–S equations. However, due to the complexity of Euler–Lagrange equation given by the action functional of the N–S equations, we do not consider such a strategy in this work and leave it to future study. Instead, we only consider to use a diagonal preconditioner. We thus need to consider the second-order variation $\delta^2 S_T(\mathbf{u}_h, p_h)$ of the action functional. Let

$$\tilde{\mathcal{N}}(\delta\tilde{\mathbf{u}}_h, \delta\tilde{\mathbf{v}}_h; \delta\mathbf{u}_h, \delta\mathbf{v}_h) = (\delta\mathbf{u}_h\cdot\nabla)\delta\tilde{\mathbf{v}}_h + (\delta\tilde{\mathbf{u}}_h\cdot\nabla)\delta\mathbf{v}_h \tag{56}$$

be the linear perturbation of the operator $\hat{\mathcal{N}}(\delta\mathbf{u}_h, \delta\mathbf{v}_h)$. The second-order variation of $S_T(\mathbf{u}_h, p_h)$ is

$$\delta^2 S_T(\mathbf{u}_h, p_h) = \langle \partial_t\delta\mathbf{u}_h - \hat{\mathcal{G}}(\delta\mathbf{u}_h, \delta p_h), \partial_t\delta\mathbf{u}_h - \hat{\mathcal{G}}(\delta\mathbf{u}_h, \delta p_h)\rangle_{\mathbf{x},t} + \langle \partial_t\mathbf{u}_h - \mathcal{G}(\mathbf{u}_h, p_h), \tilde{\mathcal{N}}(\delta\mathbf{u}_h, \delta\mathbf{u}_h; \delta\mathbf{u}_h, \delta\mathbf{u}_h)\rangle_{\mathbf{x},t}, \tag{57}$$

i.e.,

$$S_T(\mathbf{u}_h + \delta\mathbf{u}_h, p_h + \delta p_h) \approx S_T(u_h, p_h) + \delta S_T(\mathbf{u}_h, p_h) + \frac{1}{2}\delta^2 S_T(\mathbf{u}_h, p_h). \tag{58}$$

Compare Eq. (58) with the Taylor expansion of the discrete form

$$S_T(\mathbf{\Phi} + \delta\mathbf{\Phi}) \approx S_T(\mathbf{\Phi}) + \nabla S_T(\mathbf{\Phi})\delta\mathbf{\Phi} + \frac{1}{2}\delta\mathbf{\Phi}^T D^2 S_T(\mathbf{\Phi})\delta\mathbf{\Phi}, \tag{59}$$

we obtain the diagonal entries of $D^2 S_T(\mathbf{\Phi})$ using a similar procedure for the gradient $S_T(\mathbf{\Phi})$. We then define the preconditioner as the following diagonal matrix $\mathbf{P}$

$$P_{i,i} = \langle \partial_t \delta\mathbf{u}_h - \hat{\mathcal{G}}(\delta\mathbf{u}_h, \delta p_h), \partial_t \delta\mathbf{u}_h - \hat{\mathcal{G}}(\delta\mathbf{u}_h, \delta p_h)\rangle_{\mathbf{x},t}, \quad i = 1, \ldots, N_{\mathbf{x},t}, \tag{60}$$

where $\delta\mathbf{u}_h$ and δp_h are chosen as discussed in the previous section. Note that the preconditioner $\mathbf{P}$ is a function of $\mathbf{u}_h$ and p_h. Due to the well-posedness of the problem given by the linear operator $(\partial_t - \hat{\mathcal{G}})^*(\partial_t - \hat{\mathcal{G}})$, $P_{i,i}$ is positive for any given $\mathbf{u}_h$ and p_h with enough regularity.

We now present a preconditioned nonlinear CG method. Consider a new variable $\mathbf{\Phi} = \mathbf{S}\hat{\mathbf{\Phi}}$, where $\mathbf{S}$ is an invertible matrix chosen to speed up the convergence. Writing the nonlinear CG method with respect to $\hat{\mathbf{\Phi}}$ and converting it back to Φ, we obtain the preconditioned nonlinear CG method:

$$\begin{cases} \mathbf{\Phi}_{k+1} = \mathbf{\Phi}_k + \alpha_k \mathbf{d}_k, \\ \mathbf{d}_{k+1} = -\mathbf{P}\mathbf{g}_{k+1} + \bar{\beta}_k^{HZ}\mathbf{d}_k, \quad \mathbf{d}_0 = -\mathbf{P}\mathbf{g}_0, \end{cases} \tag{61}$$

where $\mathbf{P} = \mathbf{S}\mathbf{S}^{\mathrm{T}}$. The parameter $\bar{\beta}_k^{HZ}$ is the same as β_k^{HZ} except that $\mathbf{g}_k$ and $\mathbf{d}_k$ are replaced by $\mathbf{S}^{\mathrm{T}}\mathbf{g}_k$ and $\mathbf{S}^{-1}\mathbf{d}_k$, respectively. However, we do not need to know $\mathbf{S}$ explicitly by observing that $(\mathbf{S}^{\mathrm{T}}\mathbf{g}_k)^{\mathrm{T}}(\mathbf{S}^{\mathrm{T}}\mathbf{g}_k) = \mathbf{g}_k^{\mathrm{T}}\mathbf{S}\mathbf{S}^{\mathrm{T}}\mathbf{g}_k = \mathbf{g}_k^{\mathrm{T}}\mathbf{P}\mathbf{g}_k$ and $\left(\mathbf{S}^{-1}\mathbf{d}_k\right)^{\mathrm{T}}(\mathbf{S}^{\mathrm{T}}\mathbf{y}_k) = \mathbf{d}_k^{\mathrm{T}}\mathbf{S}^{-\mathrm{T}}\mathbf{S}^{\mathrm{T}}\mathbf{y}_k = \mathbf{d}_k^{\mathrm{T}}\mathbf{y}_k$. Thus we only need to know the matrix $\mathbf{P}$. Note here that for the diagonal preconditioner, we do not introduce any significant extra computational cost, since the term $\partial_t\delta\mathbf{u}_h - \hat{\mathcal{G}}(\delta\mathbf{u}_h, \delta p_h)$ required by the computation of $P_{i,i}$ has been already obtained in the computation of the gradient.

4.6. Time mesh adjustment

One difficulty of approximating the MAP is that the dynamics can significantly affect the quality of temporal discretization. Since we are looking for a curve in the phase space, we can also describe it by the arc length, i.e., the temporal discretization corresponds to an arc length discretization of the MAP. Specifically, the time element $[t_i, t_{i+1}]$ corresponds to the arc length element $[\int_0^{t_i}\sqrt{\langle\partial_t\mathbf{u}_h, \partial_t\mathbf{u}_h\rangle_{\mathbf{x}}}dt, \int_0^{t_{i+1}}\sqrt{\langle\partial_t\mathbf{u}_h, \partial_t\mathbf{u}_h\rangle_{\mathbf{x}}}dt]$. However, due to the nonlinear relation between time and arc length, a uniform discretization with respect to time may correspond to a highly nonuniform discretization with respect to arc length. For example, the time element $[t_i, t_{i+1}]$ has an element size $t_{i+1} - t_i$ while the corresponding arc length element has an element size $\int_{t_i}^{t_{i+1}}\sqrt{\langle\partial_t\mathbf{u}_h, \partial_t\mathbf{u}_h\rangle_{\mathbf{x}}}dt$, which is determined by $\partial_t\mathbf{u}_h$. In the transition region close to fixed points, the dynamics will become much slower, i.e., $\partial_t\mathbf{u}_h$ is close to zero, the arc length elements become very small and do not contribute to the approximation of the MAP. To improve the accuracy, we employ the moving mesh technique proposed in [19].

Let $s \in [0, 1]$ indicate a scaled arc length such that the total length of the MAP is equal to 1. We need to find a mapping from a temporal discretization to a (nearly) uniform discretization with respect to s. A variational approach was used in [19], which minimizes the following functional

$$E(s) = \int_0^T w^{-1}(t)\left(\frac{ds}{dt}\right)^2 dt, \tag{62}$$

where $w(t)$ is a monitor function chosen as

$$w(t) = \sqrt{1 + C\langle\partial_t\mathbf{u}_h, \partial_t\mathbf{u}_h\rangle_{\mathbf{x}}} \tag{63}$$

with C being a positive constant. Note when C goes to infinity, $w(t) \sim \|\partial_t\mathbf{u}_h\|_2$. The Euler–Lagrange equation of the functional (62) is

$$\begin{cases} \frac{d}{dt}\left(w^{-1}(t)\frac{ds}{dt}\right) = 0, \quad t \in (0, T), \\ s(0) = 0, \quad s(T) = 1. \end{cases} \tag{64}$$

For mesh adjustment, we first map the current time mesh to a discretization of $[0, 1]$ with respect to s by solving equation (64). A quadratic finite element approximation is employed. Specifically, we separate the boundary modes from the interior second-order modes. It is easy to see that the Schur complement for the boundary modes is a tridiagonal matrix which can be inversed with a linear cost. Second, we map a uniform discretization of $[0, 1]$ with respect to s to a discretization of $[0, T]$ by computing $t^{-1}(s)$. This will be our new time mesh. Third, we project the current path $(\mathbf{u}_h, p_h)$ onto the new time mesh. The

projection will be implemented element-wisely, which corresponds to inverse the mass matrix in each element and can also be done with a linear cost. More details about the mesh adjustment for MAM can be found in [23,24].

Algorithm 1. Parallel MAM for Navier–Stokes equations

Decompose the time partition $\mathcal{T}_h$ uniformly with respect to available computation nodes. Each computation node is associated with one MPI process, and deals with a sub-partition $\mathcal{T}_h^i, i = 0, \ldots, N_{\text{node}} - 1$.

Project the initial path $(\mathbf{u}, p)$ onto sub-partitions $\mathcal{T}_h^i$ of $[0, T]$ and define $\mathbf{\Phi}_0^i$ which is a vector containing all unknown coefficients related to $\mathcal{T}_h^i$.

Start the iteration of preconditioned nonlinear CG solver (61)

$$\mathbf{\Phi}_{m+1}^i = \mathbf{\Phi}_m^i + \alpha_m \mathbf{d}_m^i, \quad i = 0, \ldots, N_{\text{node}} - 1,$$

where the gradient of the action functional will be computed in parallel on each computation node by OpenMP.

Check the mesh quality very m iteration steps.

- Compute the arc length for each element according to the monitor function $w(t)$ defined in Eq. (63).
- Compute r_s^i for each sub-partition $\mathcal{T}_h^i$, which is the ratio between the largest arc length and the smallest one. If $\max_{i=0,\ldots,N_{\text{node}}-1} r_s^i$ is larger than a prescribed threshold, solve Eq. (64) to obtain a new time mesh.
- Project the current path onto the new time mesh and update $\mathbf{\Phi}_m^i$, where the projection is implemented in parallel only by MPI.

Stop the CG iteration when error tolerance or the maximum iteration number is achieved.

5. Numerical results

We study plane Poiseuille flow in the two-dimensional domain $D := [0, L] \times [-1, 1]$. Let $\alpha = 2\pi/L$. It is known that no finite- amplitude neutral (non-attenuated traveling wave) solutions exist below Reynolds number $Re \approx 2900$; for $Re \gtrsim 2900$, neutral finite-amplitude solutions exist for a finite brand of wave numbers (centred about $\alpha \simeq 1.25$ of width $\Delta\alpha \approx 0.5$ for subcritical Re); For $Re < 5772$, at any given α there are either zero or two finite-amplitude equilibria. If there are two, the lower-branch solution is unstable to two-dimensional perturbations, while the upper-branch solution is stable to all-dimensional perturbations with x-period $2\pi/\alpha$ [17]. In this section, we study the transition from the stable laminar flow to the finite-amplitude equilibrium.

5.1. Algorithm verification

To verify the algorithm, we first apply the minimum action method to two states along a certain evolution trajectory. Since there exist dynamics between these two states, the minimum action functional should be equal to zero and the corresponding MAP should recover the chosen trajectory.

We use a spectral method to solve the two-dimensional N–S equations with Fourier expansion in x direction and Legendre expansion in y direction. The temporal discretization is based on a second-order stiffly-stable scheme [14] and the velocity and pressure are updated in each time step by the influence-matrix method [2]. More details about the spectral solver is given in the appendix.

Consider initial perturbation given by the following stream function [8]

$$\psi(x, y) = k_a \left(\frac{\cosh ay}{\cosh a} - \frac{\cos ay}{\cos a} \right) \cos \theta x, \tag{65}$$

where a is a constant determined by the boundary conditions such that

$$\frac{\sinh a}{\cosh a} + \frac{\sin a}{\cos a} = 0,$$

and the constant k_a controls the degree of perturbations. We choose $L = 5.0$ and $Re = 4000$. We use 10 Fourier modes for x direction and 32 Legendre modes for y direction. For this case, a stable upper-branch solution will be obtained, which is a non-attenuated traveling wave. We then pick two states, $(\hat{\mathbf{u}}_h(\tau), \hat{p}_h(\tau))$ and $(\hat{\mathbf{u}}_h(\tau + T), \hat{p}_h(\tau + T))$, of this traveling wave as the ends of the MAP, and apply the minimum action method to the following optimization problem

$$S_T(\mathbf{u}_h^*, p_h^*) = \min_{(\mathbf{u}_h, p_h) \in A} S_T(\mathbf{u}_h, p_h), \tag{66}$$

where

$$A = \left\{ (\mathbf{u}_h(t), p_h(t)) \middle| \begin{array}{l} (\mathbf{u}_h(0), p_h(0)) = (\hat{\mathbf{u}}_h(\tau), \hat{p}_h(\tau)), \\ (\mathbf{u}_h(T), p_h(T)) = (\hat{\mathbf{u}}_h(\tau + T), \hat{p}_h(\tau + T)) \end{array} \right\}, \tag{67}$$

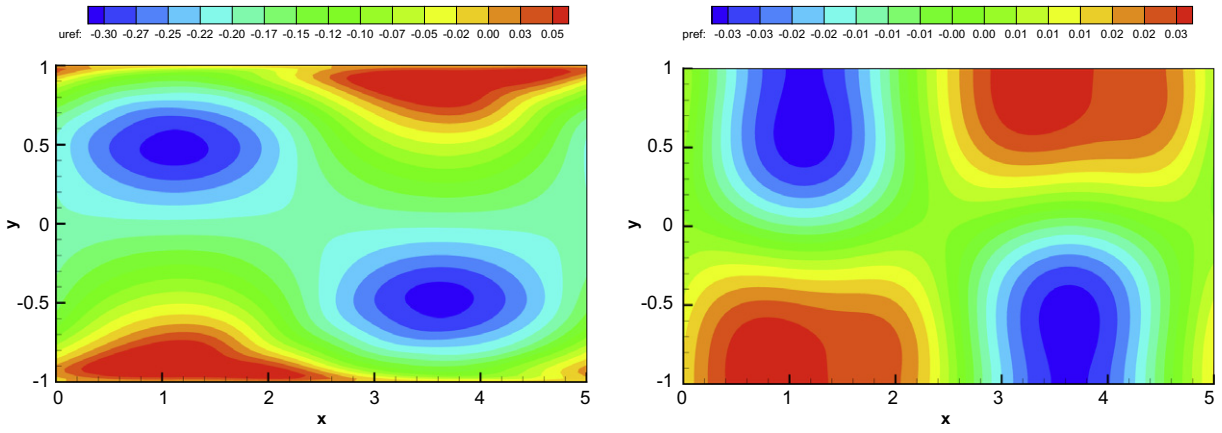

Fig. 1. Snapshots of the trajectory at time $t = 5$. Left: Horizontal velocity; Right: Pressure.

and τ is large enough such that the non-attenuated traveling wave has been well developed. We are supposed to obtain a minimizer

$$\mathbf{u}_h^*(t) = \hat{\mathbf{u}}_h(\tau + t), \quad p_h^*(t) = \hat{p}_h(\tau + t), \quad t \in [0, T],$$

such that $S_T(\mathbf{u}_h^*, p_h^*) = 0$. In Fig. 1 we plot the snapshots of horizontal velocity and pressure at $t = 5$.

Here we need to clarify one numerical issue. When solving the deterministic N–S equations numerically, the velocity field is usually obtained through the momentum equations instead of the continuity equation. For example, in the influence-matrix method, we first compute the vertical velocity and the pressure. Then we use the momentum equation rather than the continuity equation to update the horizontal velocity. Otherwise, the numerical scheme will become unstable. Hence, the obtained velocity field is not completely divergence free since the continuity equation is not explicitly satisfied while in the minimum action method the divergence-free constraint is exactly satisfied. Thus, the MAP $(\mathbf{u}_h^*, p_h^*)$ will not be completely consistent with the trajectory. Then we have

$$S_T(\mathbf{u}_h^*, p_h^*) = \hat{\epsilon}(N_t) + \epsilon(N_x, N_y) > 0,$$

where $\epsilon(N_x, N_y)$ measures the aforementioned inconsistency between the MAP $(\mathbf{u}^*, p^*)$ and the trajectory $(\hat{\mathbf{u}}_h(\tau + t), \hat{p}_h(\tau + t))$ from the divergence-free condition, and $\hat{\epsilon}(N_t)$ measures the approximation error from the temporal discretization of the MAP. Then $\hat{\epsilon} \to 0$ as $N_t \to \infty$ for some fixed N_x and N_y, and $\epsilon(N_x, N_y) \to 0$ as $N_x, N_y \to \infty$.

Assume that $\epsilon(N_x, N_y)$ is small enough such that $\hat{\epsilon}(N_t)$ is dominant. Then it is reasonable to study the convergence with respect to the temporal discretization. If we employ linear finite elements in time direction, $\hat{\epsilon}(N_t)$ should go to zero with the convergence rate $O(N_e^{-2})$, where N_e is the number of time elements. Note that such a convergence rate, in general, cannot be obtained without the time mesh adjustment. However, since the trajectory is given by a traveling wave with a certain speed,

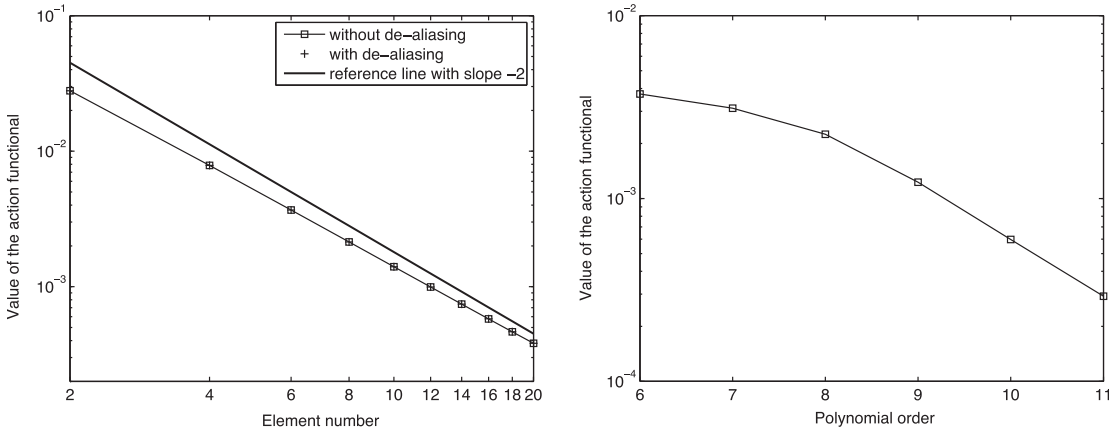

Fig. 2. Convergence of the minimum action method. Left: h-convergence of the MAP. Linear finite elements are used for the temporal discretization on the time interval $[0, T = 10]$. The reference line is a straight line with slope -2. Right: p-convergence of the MAP. One time element is used on the time interval $[0, T = 25]$.

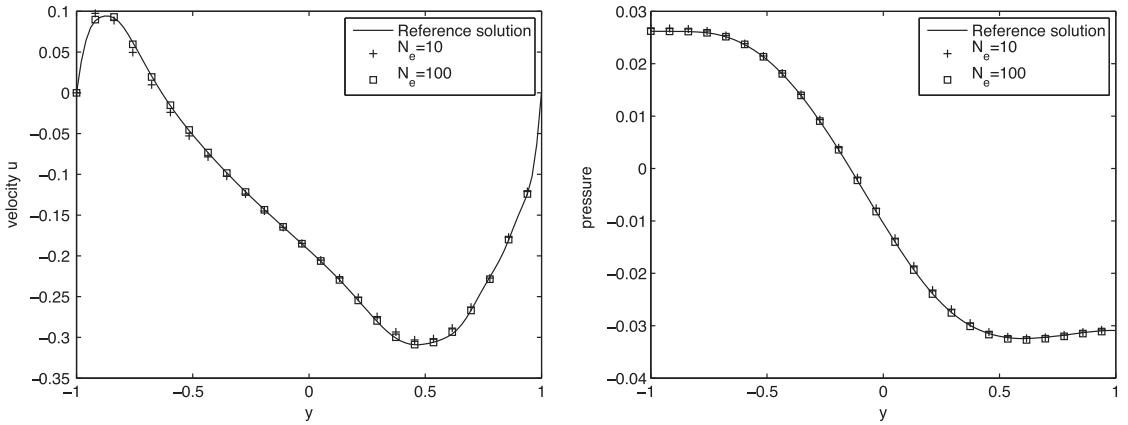

Fig. 3. Compare the MAP and the trajectory at $t = 5$ and $x = 1.2$. Left: Horizontal velocity; Right: Pressure.

the time mesh adjustment is not necessary here. In Fig. 2, we plot $S_T(\mathbf{u}_h^*, p_h^*)$ versus the number N_e of time elements on the left as the indication of h-convergence, and $S_T(\mathbf{u}_h^*, p_h^*)$ versus the polynomial order on the right as the indication of p-convergence. Due to the fast convergence we need to consider a larger time interval $[0, T = 25]$ to demonstrate the p-convergence in contrast to the time interval $[0, T = 10]$ used for the h-convergence. Furthermore, when we increase the number of quadrature points from $N_x + 1$ to $2(N_x + 1)$ in x direction and from $N_y + 3$ to $2N_y + 4$ in y direction to remove the aliasing errors, the MAP stays almost the same, which implies that the numerical solution is not sensitive to the aliasing errors for the cases studied. We subsequently compare the MAP and the trajectory at $t = 5$ and $x = 1.2$ in Fig. 3. The trajectory is computed by the aforementioned spectral solver, which has a second-order accuracy in time and the time step is chosen as 0.001. It is seen that the MAP does recover the trajectory, as expected, for both the velocity and the pressure. Finally we demonstrate the effectiveness of the diagonal preconditioner, in Fig. 4, by plotting the convergence behavior of the nonlinear CG solver with and without a preconditioner. It is seen that the diagonal preconditioner gives a speed-up of $O(10)$ for this problem.

5.2. Transition from the base flow to a traveling wave

We now present some preliminary results for the transition from the base flow to the non-attenuated traveling wave, i.e., we consider the following optimization problem

$$S_T(\mathbf{u}_{h,0\to TW}, p_{h,0\to TW}) = \min_{(\mathbf{u}_h, p_h)\in A} S_T(\mathbf{u}_h, p_h), \tag{68}$$

where

$$A = \left\{ (\mathbf{u}_h(\mathbf{x}, t), p_h(\mathbf{x}, t)) \,\middle|\, \begin{array}{l} (\mathbf{u}_h(\mathbf{x}, 0), p_h(\mathbf{x}, 0)) = (\mathbf{0}, 0), \\ (\mathbf{u}_h(\mathbf{x}, T), p_h(\mathbf{x}, T)) = (\mathbf{u}_{TW}(\mathbf{x}), p_{TW}(\mathbf{x})) \end{array} \right\}, \tag{69}$$

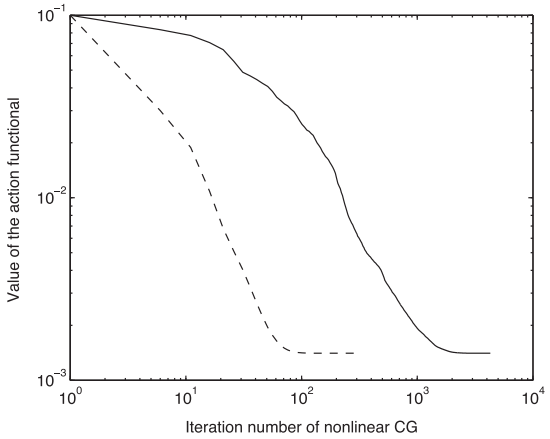

Fig. 4. Effectiveness of the diagonal preconditioner. The solid line is given by nonlinear CG without preconditioner, and the dash line is given by the same solver with the diagonal preconditioner.

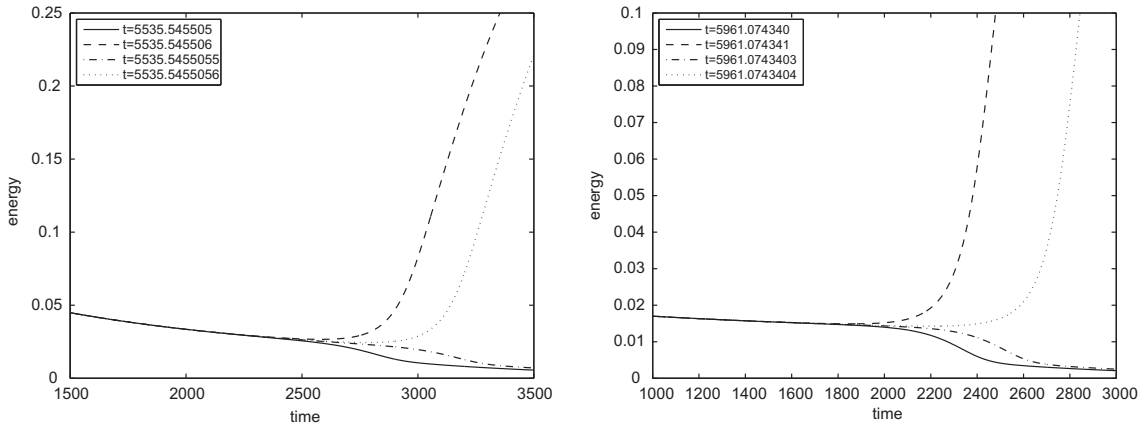

Fig. 5. Energy evolution of deterministic N–S equations starting from a certain moment of MAPs. Left: MAP $\mathbf{u}_{h,0\to TW}(t)$; Right: MAP $\mathbf{u}_{h,0\to S}(t)$.

and $(\mathbf{u}_{TW}(\mathbf{x}), p_{TW}(\mathbf{x}))$ is an arbitrary state chosen from the fully developed non-attenuated traveling wave for $L = 5$ and $Re = 4000$, and the arrow in the subscript indicates the direction of transition.

We tested two cases for problem (68) using $T = 3000, 6000$, respectively, where T is of $O(Re)$. The two cases gave consistent numerical results. We then focus on the results on the time interval $[0, 6000]$, where 3072 finite elements are used to discretize the MAP with fourth-order polynomials in each element.

The strategy to obtain a good approximation of the MAP is as follows. We first solve numerically problem (68) to obtain a MAP $\mathbf{u}_{h,0\to TW}(t), t \in [0, 6000]$, from the trivial solution to the traveling wave. We then apply a dynamic solver of N–S equations using $\mathbf{u}_{h,0\to TW}(t)$ as the initial conditions to identify the transition time $\widehat{T}$ when the dynamic solver starts to converge to the traveling wave instead of the trivial solution. In other words, at time $\widehat{T}$ the MAP exits the basin of attraction of the trivial solution. Using a bisection procedure we obtain $\widehat{T} \in (T_l = 5535.5455055, T_r = 5535.5455056)$, which means that the dynamical solver will converge to the trivial solution if the initial data is given by $\mathbf{u}_{h,0\to TW}(t), t \in [0, T_l]$, and to the traveling wave if the initial data is given by $\mathbf{u}_{h,0\to TW}(t), t \in [T_l, 6000]$. We observe that the dynamic solver of N–S equations starting from either $\mathbf{u}_{h,0\to TW}(T_l)$ or $\mathbf{u}_{h,0\to TW}(T_r)$ will first approach a state of constant energy before it diverges to the trivial solution or the traveling wave, see the left plot in Fig. 5. Furthermore, such a divergence will occur later when both T_l and T_r are more accurate. Since there exist only two stable solutions, these phenomena imply that there exist an unstable solution of N–S equations, whose unstable manifolds are connected with both the trivial solution and the traveling wave. We call this unstable saddle-like solution $\mathbf{u}_S(\mathbf{x}, t)$ the transition state, which should belong to the unstable lower-branch solutions.

Then the MAP $\mathbf{u}_{h,0\to TW}(t)$ from the trivial solution to the traveling wave can be decomposed into two parts: $\mathbf{u}_{h,0\to S}(t)$ and $\mathbf{u}_{h,S\to TW}(t)$, where the former part indicates a transition from the trivial solution to the saddle-like solution $\mathbf{u}_S(\mathbf{x}, t)$ and the latter part indicates a transition from $\mathbf{u}_S(\mathbf{x}, t)$ to the traveling wave. Since the unstable manifold of $\mathbf{u}_S(\mathbf{x}, t)$ is connected with the traveling wave, the MAP $\mathbf{u}_{h,S\to TW}(t)$ can be given by a dynamic solver of N–S equations staring from $\mathbf{u}_S(\mathbf{x}, t)$, which has a zero action. Instead of approximating the MAP $\mathbf{u}_{h,0\to TW}(t)$ directly, we can focus on $\mathbf{u}_{h,0\to S}(t)$ for a better approximation. In other words, we consider the following optimization problem

$$S_T(\mathbf{u}_{h,0\to S}, p_{h,0\to S}) = \min_{(\mathbf{u}_h, p_h)\in A} S_T(\mathbf{u}_h, p_h), \tag{70}$$

where

$$A = \left\{ (\mathbf{u}_h(\mathbf{x}, t), p_h(\mathbf{x}, t)) \middle| \begin{array}{l} (\mathbf{u}_h(\mathbf{x}, 0), p_h(\mathbf{x}, 0)) = (\mathbf{0}, 0), \\ (\mathbf{u}_h(\mathbf{x}, T), p_h(\mathbf{x}, T)) = (\mathbf{u}_S(\mathbf{x}), p_S(\mathbf{x})) \end{array} \right\}, \tag{71}$$

and the state $(\mathbf{u}_S(\mathbf{x}), p_S(\mathbf{x}))$ are approximated by the state of the lowest energy on the trajectory given by the dynamic solver starting from $\mathbf{u}_{h,0\to TW}(T_r)$. Using the same parameters, we compute $\mathbf{u}_{h,0\to S}(t)$ on time interval $[0, 6000]$. A similar decomposition can be implemented to obtain the transition time $\widehat{T} \in (T_l = 5961.0743403, T_r = 5961.0743404)$ on the MAP $\mathbf{u}_{h,0\to S}(t)$ since the approximated state $\mathbf{u}_S(\mathbf{x})$ is out of the basin of attraction of the trivial solution. Energy evolution of the dynamic solver starting from a certain moment of the MAP $\mathbf{u}_{h,0\to S}(t)$ is given in the right plot of Fig. 5, where we see that the saddle-like solution $\mathbf{u}_S(\mathbf{x}, t)$ has an energy about 0.0143. Snapshots of the approximated state $\mathbf{u}_S(\mathbf{x})$ are give in Fig. 6. We note that the saddle-like solution $\mathbf{u}_S(\mathbf{x}, t)$ has a similar profile with the traveling wave solution, see Figs. 1 and 6, while the traveling wave solution is stable with a much larger energy 0.347.

To this end, we see that the saddle-like solution $\mathbf{u}_S(\mathbf{x}, t)$ should be located on the separatrix of the trivial solution and the traveling wave solution, and plays a critical role for the transition. When the transition occurs, the MAP goes through the basin of attraction of the trivial solution through $\mathbf{u}_S(\mathbf{x}, t)$.

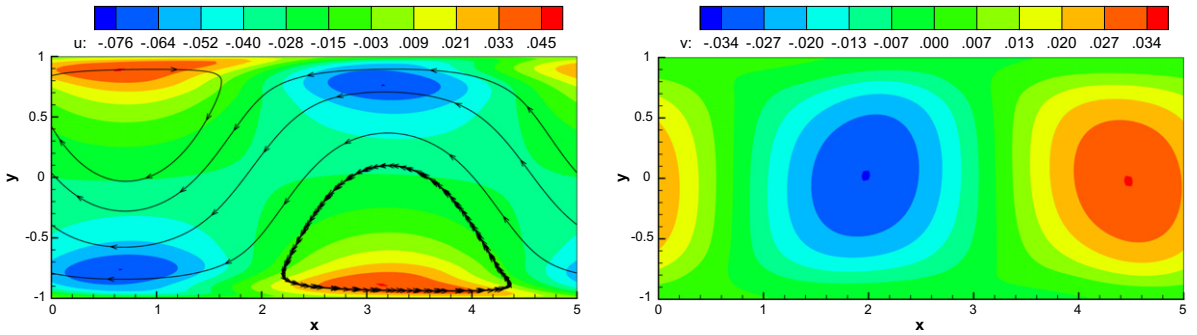

Fig. 6. Snapshots of the transition state on the MAP. Left: Horizontal velocity with streamlines; Right: Vertical velocity.

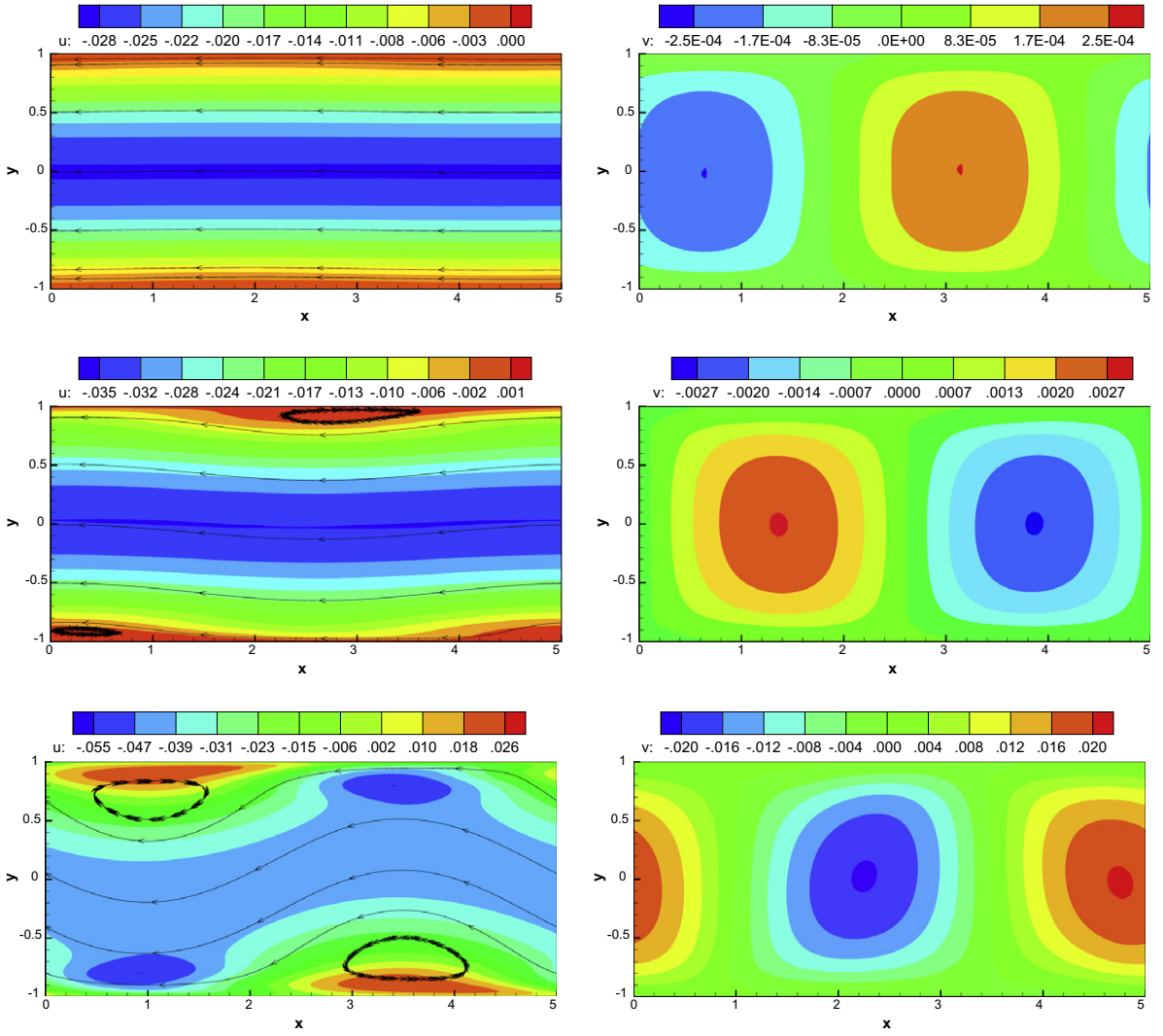

Fig. 7. Snapshots of flow field on the MAP $\mathbf{u}_{h,0\to S}(t)$. We regard each plot (a_{ij}) as one entry of a matrix, $i = 1, 2, 3,\ j = 1, 2$. Each row corresponds to time $t = 5000, 5400, 5800$ from top to bottom. The left column consists of snapshots of horizontal velocity with streamlines. The right column consists of snapshots of vertical velocity.

We now examine the evolution of $\mathbf{u}_{h,0\to S}(t)$ on the time interval $[0, T_r = 5961.0743404]$. In Fig. 7 we plot snapshots of horizontal and vertical velocities on the MAP $\mathbf{u}_{h,0\to S}(t)$ at time $t = 5000, 5400, 5800$, where the range of the contours are from the

minimum to the maximum of the corresponding velocity component. It is observed that up to time $t = 5000$, the disturbance is almost a parallel shear flow since the vertical velocity is much smaller than the horizontal velocity. The effect of the disturbance with negative horizontal velocity is mainly to slow down the base flow. As the amplitude of the vertical velocity increases, the oscillation becomes stronger until boundary layer instability occurs and two vortices emerge from boundaries (one from the top boundary and the other one from the bottom boundary). As the amplitude of the oscillation keeps increasing, the two vortices are also strengthened. Eventually the saddle-like solution $\mathbf{u}_S(\mathbf{x}, t)$ is reached when the transition occurs. Since the MAP $\mathbf{u}_{h,0\to S}(t)$ is the least unlikely path for the transition from the trivial solution to $\mathbf{u}_S(\mathbf{x}, t)$, the above observations provide the most probable scenario that the disturbance develops from zero to a critical state for instability to occur.

6. Summary

In this work, we developed a parallel minimum action method for small random perturbations of Navier–Stokes equations. The optimization problem given by the Freidlin–Wentzell least action principle is transformed to an unconstrained one by taking care of the boundary conditions and the incompressibility condition explicitly, which is then solved by a preconditioned nonlinear conjugate gradient solver. The algorithm is verified by examining a non-attenuated traveling wave in the two- dimensional Poiseuille flow, where both h- and p-convergence are obtained and it is also observed that the MAP can recover the trajectory of both velocity and pressure if there exists dynamics between the two given states. We also presented some preliminary results for the nonlinear instability of the two-dimensional Poiseuille flow.

There are many open problems and possibilities generated by this work from both numerical and application point of view. (1) In this work we used spectral discretization in physical space, which implicitly deals with the different regularity requirements given by the original PDE and the Euler–Lagrange equation of the Freidlin–Wentzell action functional. For a general finite element discretization in physical space, such an issue will be taken care of by either a different construction of the finite element basis or a modification of the discretization of the Freidlin–Wentzell action functional; (2) One important numerical issue is the improvement of the diagonal preconditioner; (3) As for the application to nonlinear instability, a much more interesting and important problem is to apply the developed algorithm to look for the characteristic features of the transition of parallel shear flows in both two- and three-dimensional long channels.

Acknowledgments

This work was supported by DOE Grant SC0002324 and NSF Grant DMS-1115632. The parallel computation was implemented on supercomputers supported by the Louisiana Optical Network Institute (LONI).

Appendix A. A spectral solver for the Navier–Stokes equations

Since the channel flow has a simple geometry, we consider the spectral method to solve the N–S equations with Fourier expansion in x direction and Legendre expansion in y direction. The problem is defined as:

$$\begin{cases} \frac{\partial \mathbf{u}}{\partial t} + (\mathbf{u}_{\text{tot}} \cdot \nabla)\mathbf{u}_{\text{tot}} = -\nabla p + \frac{1}{Re}\Delta \mathbf{u}, \\ \nabla \cdot \mathbf{u} = 0 \end{cases} \tag{A.1}$$

with boundary conditions

$$\begin{cases} \mathbf{u}|_{x=0} = \mathbf{u}|_{x=L}, \\ p|_{x=0} = p|_{x=L}, \\ \mathbf{u}|_{y=\pm \mathrm{h}} = 0. \end{cases} \tag{A.2}$$

For the temporal discretization we use the stiffly-stable scheme [14]:

$$\frac{\gamma_0 \mathbf{u}^{n+1} - \sum_{q=0}^{J_i-1} \alpha_q \mathbf{u}^{n-q}}{\Delta t} = -\nabla p^{n+1} - \sum_{q=0}^{J_e-1} \beta_q \mathcal{N}(\mathbf{u})^{n-q} + \nu \mathcal{L}(\mathbf{u}^{n+1}), \tag{A.3}$$

with

$$\mathcal{N}(\mathbf{u}) = (\mathbf{u}_{\text{tot}} \cdot \nabla)\mathbf{u}_{\text{tot}}, \quad \mathcal{L}(\mathbf{u}) = \Delta \mathbf{u},$$

where J_i and J_e are integration orders for the diffusion term and the advection term, respectively, and the coefficients γ_0, α_q and β_q are determined by the accuracy order of the numerical scheme [14]. For the spatial discretization, we use Fourier expansion in the x direction and Legendre expansion in the y direction. For x direction, the Fourier expansion is employed for both $\mathbf{u}$ and p because of the periodic boundary conditions. Considering the constraint $\mathbf{u}|_{y=\pm \mathrm{h}} = 0$, we choose the basis functions for the y direction as $P_m(y/\mathrm{h}) - P_{m+2}(y/\mathrm{h})$ for the velocity $\mathbf{u}$, and $P_m(y/\mathrm{h})$ for the pressure p, where $P_m(y)$ is the Legendre polynomial of order m. Then we have the following approximation

$$\mathbf{u} \approx \mathbf{u}_h = \sum_{i=0}^{N_y} \mathbf{u}_i(x,t)(P_m(y/\mathrm{h}) - P_{m+2}(y/\mathrm{h})), \tag{A.4}$$

$$p \approx p_h = \sum_{i=0}^{N_y+1} p_i(x,t) P_m(y/\mathrm{h}), \tag{A.5}$$

where the highest polynomial order for velocity is $N_y + 2$ while the highest polynomial order for pressure is $N_y + 1$. This is due to the fact that $P_{N_y+2}(y/\mathrm{h})$ is a spurious mode for the pressure. Also note that the mean of the pressure should be equal to zero, i.e. $\int_D p d\mathbf{x} = 0$.

We re-organize the Eq. (A.1) as

$$\nu \Delta \mathbf{u}^{n+1} - \lambda \mathbf{u}^{n+1} - \nabla p^{n+1} = -\mathbf{R}^n, \tag{A.6}$$

where

$$\lambda = \gamma_0/\Delta t,$$
$$\mathbf{R}^n = \frac{1}{\Delta t}\sum_{q=0}^{J_i-1} \alpha_q \mathbf{u}^{n-q} - \sum_{q=0}^{J_e-1} \beta_q \mathcal{N}(\mathbf{u})^{n-q}.$$

Then for each Fourier mode $e^{\mathbf{i}k\frac{2\pi}{L}x}$, we have the following equations in the Fourier space

$$\nu \hat{\mathbf{u}}'' - (\nu\theta_k^2 + \lambda)\hat{\mathbf{u}} - \hat{\nabla}\hat{p} = -\hat{\mathbf{R}}, \tag{A.7}$$

$$\hat{\nabla}\cdot\hat{\mathbf{u}} = 0, \tag{A.8}$$

$$\hat{\mathbf{u}}(\pm\mathrm{h}) = 0, \tag{A.9}$$

where we drop subscript k and time level $n+1$ for all Fourier coefficients, the prime indicates the derivative with respect to y, and

$$\theta_k = k\frac{2\pi}{L} \tag{A.10}$$

$$\hat{\nabla}\hat{p}^{n+1} = (\mathbf{i}\theta_k \hat{p}^{n+1}, \partial\hat{p}^{n+1}/\partial y), \tag{A.11}$$

$$\hat{\nabla}\cdot\hat{\mathbf{u}}^{n+1} = \mathbf{i}\theta_k\hat{u}^{n+1} + \partial\hat{v}^{n+1}/\partial y. \tag{A.12}$$

Taking the divergence of (A.7) and applying the divergence-free constraint, we have the equation for the pressure

$$\hat{p}'' - \theta_k^2\hat{p} = \hat{\nabla}\cdot\hat{\mathbf{R}}, \tag{A.13}$$

subject to the boundary conditions

$$\hat{\nabla}\cdot\hat{\mathbf{u}}(\pm\mathrm{h}) = 0, \quad \text{i.e.,} \hat{v}'(\pm\mathrm{h}) = 0. \tag{A.14}$$

The momentum equation for $\hat{v}$ and $\hat{u}$ are

$$\nu\hat{v}'' - (\nu\theta_k^2 + \lambda)\hat{v} - \hat{p}' = -\widehat{R}_y, \quad \hat{v}(\pm\mathrm{h}) = 0, \tag{A.15}$$

$$\nu\hat{u}'' - (\nu\theta_k^2 + \lambda)\hat{u} - \mathbf{i}\theta_k\hat{p} = -\widehat{R}_x, \quad \hat{u}(\pm\mathrm{h}) = 0. \tag{A.16}$$

To solve Eqs. (A.13)–(A.16), we employ the influence-matrix method [2]. Eqs. (A.13)-(A.15) are called "A-Problem" and the following equations "B-Problem":

$$\hat{p}'' - \theta_k^2\hat{p} = \hat{\nabla}\cdot\hat{\mathbf{R}}, \quad \hat{p}(\pm\mathrm{h}) = \hat{p}_\pm, \tag{A.17}$$

$$\nu\hat{v}'' - (\nu\theta_k^2 + \lambda)\hat{v} - \hat{p}' = -\widehat{R}_y, \quad \hat{v}(\pm\mathrm{h}) = 0. \tag{A.18}$$

The pressure $\hat{p}_\pm$ at the walls are unknown a priori, but it is required to be consistent with the conditions $\hat{v}'(\pm\mathrm{h}) = 0$. Let $(\hat{p}_p, \hat{v}_p)$ be the solution of Eqs. (A.17) and (A.18) but with homogeneous Dirichlet boundary conditions on $\hat{p}$. Let $(\hat{p}_+, \hat{v}_+)$ and $(\hat{p}_-, \hat{v}_-)$ be the solutions of the homogeneous B-Problems with zero on the right-hand sides of differential equations, with boundary conditions $\hat{p}_+(-\mathrm{h}) = 0$, $\hat{p}_+(\mathrm{h}) = 1$, and $\hat{p}_-(-\mathrm{h}) = 1$, $\hat{p}_-(\mathrm{h}) = 0$, respectively. Write the solution of the A-Problem as

$$\begin{pmatrix}\hat{p}\\ \hat{v}\end{pmatrix} = \begin{pmatrix}\hat{p}_p\\ \hat{v}_p\end{pmatrix} + \delta_+\begin{pmatrix}\hat{p}_+\\ \hat{v}_+\end{pmatrix} + \delta_-\begin{pmatrix}\hat{p}_-\\ \hat{v}_-\end{pmatrix}. \tag{A.19}$$

The boundary conditions of the A-Problem require

$$\begin{pmatrix}\hat{v}'_+(+\mathrm{h}) & \hat{v}'_-(+\mathrm{h})\\ \hat{v}'_+(-\mathrm{h}) & \hat{v}'_-(-\mathrm{h})\end{pmatrix}\begin{pmatrix}\delta_+\\ \delta_-\end{pmatrix} = -\begin{pmatrix}\hat{v}'_p(+\mathrm{h})\\ \hat{v}'_p(-\mathrm{h})\end{pmatrix}. \tag{A.20}$$

This determines δ_+ and δ_-, and hence the correct pressure boundary condition is

$$\hat{p}(\pm \mathsf{h}) = \delta_{\pm}.$$

For each time step, the *B*-Problem is first solved with homogeneous pressure boundary conditions, and then solved again using the correct pressure boundary conditions. Having $\hat{p}$ and $\hat{v}$, then $\hat{u}$ will be obtained from the momentum equation instead of the continuity equation for the reason of numerical stability.

References

[1] C.J. Cerjan, W.H. Miller, On finding transition states, J. Chem. Phys. 75 (6) (1981) 2800–2806.
[2] C. Canuto, M.Y. Hussaini, A. Quarteroni, T.A. Zang, Spectral Methods in Fluid Dynamics, Springer-Verlag, 1988.
[3] W. E, W. Ren, E. Vanden-Eijnden, String method for the study of rare events, Phys. Rev. B 66 (2002) 052301.
[4] W. E, W. Ren, E. Vanden-Eijnden, Minimum action method for the study of rare events, Commun. Pure Appl. Math. 57 (2004) 565–637.
[5] W. E, W. Ren, E. Vanden-Eijnden, Simplified and improved string method for computing the minimum energy paths in barrier-crossing events, J. Chem. Phys. 126 (2007) 164103.
[6] W.G. Faris, G. Jona-Lasinio, Large fluctuations for a nonlinear heat equation with noise, J. Phys. A Math. Gen. 15 (1982) 3025–3055.
[7] M.I. Freidlin, A.D. Wentzell, Random Perturbations of Dynamical Systems, second ed., Springer-Verlag, New York, 1998.
[8] W.D. George, J.D. Hellums, B. Martin, Finite-amplitude neutral disturbances in plane Poiseuille flow, J. Fluid Mech. 63 (1974) 765–771.
[9] W.W. Hager, H. Zhang, A new conjugate gradient method with guaranteed descent and an efficient line search, SIAM J. Optim. 16 (1) (2005) 170–192.
[10] M. Heymann, E. Vanden-Eijnden, The geometric minimum action method: a least action principle on the space of curves, Commun. Pure Appl. Math. 61 (2008) 1052–1117.
[11] G. Henkelman, H. Jónsson, A dimer method for finding saddle points on high dimensional potential surfaces using only first derivatives, J. Chem. Phys. 111 (15) (1999) 7010–7022.
[12] H. Jònsson, G. Mills, K.W. Jacobsen, Nudged elastic band method for finding minimum energy paths of transitions, in: B. Berne, G. Ciccotti, D. Coker (Eds.), Classical and Quantum Dynamics in Condensed Phase Simulations, 1998.
[13] N.G. van Kampen, Stochastic Processes in Physics and Chemistry, North-Holland, 1981.
[14] G.E. Karniadakis, S.J. Sherwin, Spectral/hp Element Methods for Computational Fluid Dynamics, second ed., Oxford University Press, 2005.
[15] A. Monokrousos, A. Bottaro, L. Brandt, A. Di Vita, D.S. Henningson, Nonequilibrium thermodynamics and the optimal path to turbulence in shear flows, Phys. Rev. Lett. 106 (2011) 134502.
[16] L. Onsager, S. Machlup, Fluctuations and irreversible processes, Phys. Rev. 91 (1953) 1505–1512.
[17] S. Orszag, A. Patera, Secondary instability of wall-bounded shear flows, J. Fluid Mech. 128 (1983) 347–385.
[18] S.S. Sritharan, P. Sundar, Large deviations for the two-dimensional Navier–Stokes equations with multiplicative noise, Stochastic Process. Appl. 116 (2006) 1636–1659.
[19] X. Zhou, W. Ren, W. E, Adaptive minimum action method for the study of rare events, J. Chem. Phys. 128 (2008) 104111.
[20] X. Zhou, W. E, Study of noise-induced transitions in the Lorenz system using the minimum action method, Commun. Math. Sci. 8 (2) (2010) 341–355.
[21] W. Ren, Numerical Methods for the Study of Energy Landscape and Rare Events, Ph.D thesis, New York University, 2002.
[22] X. Wan, X. Zhou, W. E, Study of the noise-induced transition and the exploration of the configuration space for the Kuramoto–Sivashinsky equation using the minimum action method, Nonlinearity 23 (2010) 475–493.
[23] X. Wan, An adaptive high-order minimum action method, J. Comput. Phys. 230 (2011) 8669–8682.
[24] X. Wan, G. Lin, Hybrid parallel computing of minimum action method, Parallel Comput., submitted for publication.